

# Direct ab initio calculation of magnons in altermagnets: method, spin-space symmetry aspects, and application to MnTe

L. M. Sandratskii<sup>1,2\*</sup>, K. Carva<sup>1</sup>, V. M. Silkin<sup>2,3,4</sup>

<sup>1</sup>*Faculty of Mathematics and Physics,  
Charles University, 12116 Prague, Czech Republic*

<sup>2</sup>*Donostia International Physics Center (DIPC),  
Paseo de Manuel Lardizabal 4,  
E-20018 San Sebastián, Spain*

<sup>3</sup>*Departamento de Polímeros y Materiales Avanzados: Física,  
Química y Tecnología, Facultad de Ciencias Químicas,  
Universidad del País Vasco (UPV-EHU),  
Apdo. 1072, E-20080 San Sebastián, Spain*

<sup>4</sup>*IKERBASQUE, Basque Foundation for Science,  
48011 Bilbao, Spain*

We suggest the method for direct ab initio calculation of magnons in complex collinear magnets. The method is based on the density-functional-theory (DFT) calculation under two different constraints: one constraint governs the change of the magnetization with respect to the ground state, and the other is the symmetry constraint responsible for the value of the magnon wave vector. The performance of the method is demonstrated by the application to an altermagnet MnTe. An important role in both the formulation and the application of the method play the aspects of generalized symmetry described by the spin-space groups. The symmetry analysis connects in one coherent picture the following three parts of the consideration: (i) the generalized translational symmetry of the magnons as a crucial condition for their efficient ab-initio calculation, (ii) altermagnetic spin-splitting of the electron states in the ground magnetic state, and (iii) chirality splitting of the magnon excitations. It is demonstrated that both the spin splitting of the electron states and the chirality splitting of the magnons, though very different in their physical nature, have identical patterns in the corresponding wave vector spaces. Since the altermagnetism of MnTe is the consequence of the presence of the Te atoms, an adequate attention is devoted to the symmetry analysis and calculation results for the Te moments induced in the magnon states. The knowledge on the symmetry properties of the Te moments allows to accelerate the numerical convergence of the magnon states and serves as a test for the accuracy of the calculations. To expose the connection between electron band structures of the magnon states of the system and the chirality properties of these states we investigate the transformation of the electron structure in the transition from the collinear ground state to a noncollinear magnon state.

PACS numbers:

## I. INTRODUCTION

Magnons as low energy excitations of the magnetic systems play a central role in the the magnetic thermodynamics. The emerging field of magnonics enhanced further the importance of the magnons<sup>1-4</sup>. The first-principles study of the magnons is one of the prominent tasks of the theoretical approaches to magnetic systems based on the density functional theory (DFT).

In the adiabatic picture focusing on the dynamics of atomic magnetic moments, the magnons are presented by the configurations of the moments deviating from the magnetization axis<sup>5-7</sup>. The structure of a magnon is characterized by the wave vector and by the angles specifying the deviation of the atomic moments from the magnetization axis. For an elemental ferromagnet (FM) with

one magnetic atom per the crystallographic unit cell the structure of the magnons is uniquely determined by the wave vector [Fig. 1(a)]. The deviation angle  $\theta$  is the same for all atoms. Therefore in this case only the energies of the magnons need to be determined. In more complex systems such as antiferromagnets (AFM) [Fig. 1(b),(c)], ferrimagnets, or ferromagnets with several inequivalent atoms in the crystallographic unit cell, different atomic moments deviate differently from the magnetization axis and the determination of the structure of the magnons is an important part of the magnon study.

There are different approaches to the DFT based calculation of magnons. One of the approaches is the calculation of the dynamic magnetic susceptibility in nonuniform transversal magnetic field<sup>8-14</sup>. A strong feature of this method is that it allows to investigate not only the structure and the energy of magnons but also their life time resulting from the interaction of magnons with single-electron Stoner excitations. In the case of complex magnetic materials the method is very demanding

---

\*lsandr3591@gmail.com

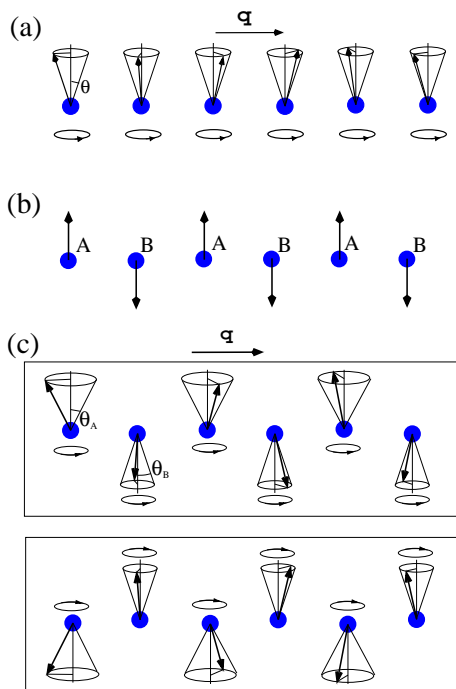


FIG. 1: (a) Schematic presentation of the spin waves in an elemental ferromagnet. (b) Schematic presentation of the ground state magnetic structure of a two sublattice AFM. Sublattices are marked by letters A and B. (c) Schematic presentation of the spin waves in a two sublattice AFM. Angles  $\theta_A$  and  $\theta_B$  give deviations of the atomic moments of the sublattices from the magnetization axis. Upper part: magnon of type A with  $\theta_A > \theta_B$ . Lower part: magnon of type B with  $\theta_B > \theta_A$ .

with respect to both computation techniques and computer resources. A widely used approach to the theoretical study of the adiabatic magnons is the mapping, as an intermediate step, of the electron system on the Heisenberg Hamiltonian of interacting atomic moments. Such a mapping is currently a standard procedure consisting in the DFT based evaluation of the Heisenberg exchange parameters (see, e.g., Refs. 15–22). An efficient method of the mapping was suggested by Liechtenstein et al.<sup>15</sup> and is based on the evaluation of the variation of the band energy as the response to the infinitesimal deviation of the atomic moments from the magnetization axis. The possibility to replace the variation of the total energy by the variation of the band energy is based on so-called magnetic force theorem<sup>15</sup>. A recent review of the development and applications of the Liechtenstein et al. method is given in Ref. 23. In this paper we suggest a direct DFT-based method for the magnon calculation that does not include mapping of the electron system on the Heisenberg Hamiltonian.

The direct method needs more computer time than the mapping procedure by Liechtenstein et al. since each magnon state is calculated in a separate self-consistent DFT calculation. However, the method has features not provided by the standard mapping approach. Among

them are the following: First, the fully self-consistent calculation of the magnon structure and energy is performed in contrast to the mapping approach based on the evaluation of the band energy variation from non self-consistent calculation. Second, in the magnon states of complex structures the atoms that are equivalent in the ground state may become inequivalent. The suggested method takes this into account in a consequent self-consistent manner. Third, in the compounds the contribution of the nominally nonmagnetic atoms to the magnon states is self-consistently taken into account. Forth, the method allows to estimate the dependence of the magnon energy on the number of magnons by varying the tilting angles of the atomic moments from the magnetization axis. The approach suggested by Liechtenstein et al. considers an infinitesimal deviation of the moments from the magnetization axis.

Since each magnon presents a different state of the system, the direct self-consistent calculation of a magnon state within the DFT framework must include constraints responsible for the convergence of the calculation to the desired magnetic state instead of the standard DFT convergence to the ground state (GS). Two different constraints are simultaneously used in the method. The first governs the change of the net magnetization. The method uses the formula

$$\omega = \frac{\Delta E}{\Delta m_z} \quad (1)$$

derived in Ref. 7 for the magnon energy in an arbitrary collinear magnet. Here  $\Delta E$  is the increase of the energy of the magnon state with respect to the GS and  $\Delta m_z$  is the magnetization change with respect to the GS magnetization. Equation (1) correlates with the property that one magnon changes the magnetization of the system by  $1 \mu_B$ . The first constraint imposes the condition on the magnetization of the system by means of introduction of an effective magnetic field. The second constraint specifies the value of the magnon wave vector. This is a symmetry type of constraint<sup>24</sup> where the invariance of the initial Hamiltonian with respect to the symmetry operation responsible for the desired property reproduces itself during iterations. The symmetry constraint does not need a constraining field. It is important to emphasize that to constrain the magnon wave vector the generalized translational periodicity described by the machinery of spin space groups (SSG) must be imposed.

In the paper, we formulate the method in the form valid for the study of the magnons in any collinear magnet with weak spin-orbit coupling (SOC). The performance of the method is demonstrated by the application to altermagnets focusing on MnTe as a representative of this class of materials. As the notion of an altermagnet is rather new it is worth to introduce it briefly. The ground state of a two sublattice AFM is characterized by two mutually compensating ferromagnetic sublattices. In terms of the electron structure, the zero net magnetization of an AFM is the result of the mutual compensation of the

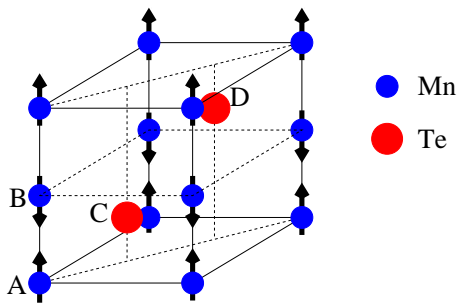


FIG. 2: Unit cell of AFM MnTe. Labeling A-D of the sublattices is used throughout the paper.

spin-up and spin-down electron states which is the consequence of the symmetry properties of the material. Importantly, the realization of this spin compensation can be different for different AFM materials: It can take place either at each wave vector  $\mathbf{k}$  of the reciprocal space or, alternatively, between the electron states corresponding to different  $\mathbf{k}$  points. Šmejkal, Sinova, and Jungwirth<sup>25,26</sup> suggested the term *altermagnet* for the materials where the magnetic compensation takes place between different  $\mathbf{k}$  points. The absence of the spin degeneracy at the same  $\mathbf{k}$  point can be treated as the spin splitting of the electron states at this point. This property of altermagnets has important physical consequences attracting considerable research attention to this class of materials<sup>26–32</sup>.

Among the special properties of altermagnets is the chirality splitting of the magnon states<sup>22,28,33,34</sup>. Each AFM magnon brings either positive or negative magnetization to the system. If in Fig. 1(c)  $\theta_A > \theta_B$  the magnon gives negative contribution to the magnetization whereas for a magnon with  $\theta_A < \theta_B$  the contribution to the magnetization is positive. These two types of magnons have opposite chiralities. The two types of magnons are obtained in both Heisenberg model (see, e.g., Ref. 35) and first-principles calculation of the dynamical spin susceptibility (see, e.g., Ref. 10). We will refer to these two types of magnons as magnons of type A and B according to the larger of two angles  $\theta_A$  and  $\theta_B$ . The net magnetization of an AFM at nonzero temperatures remains zero. This property is the consequence of the mutual compensation of the magnons of opposite chiralities which results from their symmetry-determined energy degeneracy. Again there are two possibilities. The chirality compensation can take place either at each magnon wave vector  $\mathbf{q}$  or only between magnons with different wave vectors. The latter situation takes place in altermagnets and may be referred to as chirality splitting of magnons with a given wave vector  $\mathbf{q}$ . The nature of the chirality degeneracy of the magnons is very different compared to the spin degeneracy of the electron states discussed above. However, in both cases the two symmetry questions to address are similar: First, which symmetry operations are responsible for the degeneracy of the magnons with opposite chiralities, and, second, does the degeneracy take place

between the magnons with the same wave vector or with different wave vectors? As will be discussed, the answers to these questions for magnons are closely related to those for the electron states.

Our choice of altermagnet MnTe as the object of the application of the method has following reasons. First, as a particular case of a two-sublattice AFM containing nonmagnetic atoms (Fig. 2) it is complex enough to demonstrate important features of the method. In the case of MnTe, the altermagnetic properties are the consequences of the presence of the Te atoms. Indeed, in an assumed material with removed Te atoms the altermagnetic spin and chirality splittings are absent. Because of the importance of the Te atoms for the altermagnetism the account for their self-consistent response to the changes in the Mn subsystem is an important feature. In this respect, among the questions to address are, first, whether the Te atoms remain equivalent in the magnon states and, second, what can be said about induced Te moments on the basis of symmetry arguments? The magnon-specific symmetry information about nonmagnetic atoms helps to control and accelerate the convergence of the magnon calculation.

Next question addressed in the paper is how the chirality properties of the magnon states of the system are related to the properties of the electron band structures of these states. The deep connection between two different energy characteristics is exposed.

As seen from the above, the symmetry aspects play in the paper an important role. There are three different parts of the work where the symmetry arguments are essential: (i) the formulation of the method of the direct magnon calculation, (ii) the study of the spin-splitting of the electron states in the GS of an altermagnet, and (iii) the study of the chirality-splitting of the spin waves in an altermagnet. The employment of the SSG allows both solving these tasks and the integration of different parts of the study in one coherent physical picture.

The paper is structured as follows. In Sec. II the method of direct DFT based calculation of magnon states is presented. Section III gives the details of the calculations. In Sec. IV the symmetry aspects and the results of the calculations are discussed. This section includes a brief introduction of the SSGs (Sec. IV A), discussion of the spin degeneracy and altermagnetic spin-splitting of the electron states in AFM (Sec. IV B), application to the electron states of MnTe (Sec. IV C), discussion of the symmetry governed properties of the magnetic sublattices in the magnon states (Sec. IV D) and of the chirality splitting of magnons in altermagnets (Sec. IV E), results of the calculation of magnon dispersion (Sec. IV F), brief discussion of the noticed instability cases of magnon state energy with respect to the number of magnons (Sec. IV G), and the study of the relation between electronic band structures of the magnon states and chirality properties of these states (Sec. IV H). Section V is devoted to the conclusions.

## II. THE METHOD OF DIRECT DFT-BASED MAGNON CALCULATION

As mentioned in the introduction, in Ref. 7 it was shown that for any collinear magnet the magnon energy can be calculated applying Eq. (1). The value of  $\Delta m_z$  corresponds to the number of magnons with given wave vector and  $\Delta E$  is their energy. It is expected that there is an interval of  $\Delta m_z$  where  $\Delta E$  is proportional to  $\Delta m_z$  and the calculation for any  $\Delta m_z$  from this interval gives the value of the spin wave energy. The both quantities can be taken per unit cell. To obtain the self-consistent magnon state with a given magnetization  $m_o - \Delta m_z$  the minimization of the density functional must be performed under the constraining condition

$$\int d\mathbf{r} m_z(\mathbf{r}) = m_o - \Delta m_z. \quad (2)$$

Here  $m_o$  is the ground state magnetization that is zero in the case of an AFM.

The constrained energy functional takes the form

$$E_{const}[n, \mathbf{m}] = E[n, \mathbf{m}] + h \left[ \int d\mathbf{r} m_z(\mathbf{r}) - m_o + \Delta m_z \right] \quad (3)$$

where  $E[n, \mathbf{m}]$  is unconstrained functional, Lagrange parameter  $h$  plays the role of the  $z$  component of an effective magnetic field  $\mathbf{h} = (0, 0, h)$ . The condition on the magnetization [Eq. (2)] is the same for all magnons independent of their wave vectors whereas the value of field  $h$  corresponding to a given  $\Delta m_z$  is  $\mathbf{q}$  dependent. In systems with well defined atomic moments considered in the paper, field  $\mathbf{h}$  governs the values of the deviations of the moments from the  $z$  axis. For each magnetic atom, the vector of the constraining field  $\mathbf{h}$  can be decomposed into two components: one collinear to the moment and the other orthogonal to it (Fig. 3). The component collinear to the moment influences the value of the moment. This influence is weak for well defined atomic moments since the variation of the value of the moments is energetically costly. In this case the orthogonal component plays the main role governing the deviation of the moments from the magnetization axis and leading to the desired magnetization change  $\Delta m_z$ . The orthogonal components form nonuniform magnetic field with wavelength identical to the wavelength of the magnon.

The second constraint specifying the wave vector  $\mathbf{q}$  of the magnon reflects the generalized periodicity<sup>36</sup> of the helix with given  $\mathbf{q}$

$$\{\alpha_{\mathbf{q}n} | E | \mathbf{R}_n \} \mathbf{m}(\mathbf{r}) \equiv \alpha_{\mathbf{q}n} \mathbf{m}(\mathbf{r} - \mathbf{R}_n) = \mathbf{m}(\mathbf{r}) \quad (4)$$

Here  $\{\alpha_{\mathbf{q}n} | E | \mathbf{R}_n \}$  are the operators of generalized translations consisting from the lattice translation  $\mathbf{R}_n$  accompanied by the rotation of magnetization by angle  $\mathbf{q}\mathbf{R}_n$  about the  $z$  axis.  $E$  in the second position in the symmetry operator means that the operator does not perform any point transformation besides the magnetization rotation. The Kohn-Sham equation of a helical structure

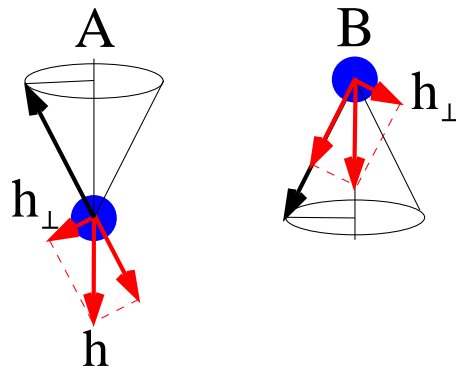


FIG. 3: Schematic picture of the decomposition of the constraining field  $\mathbf{h}$  into two components: one collinear to the moment and the other,  $\mathbf{h}_\perp$ , orthogonal to it. The left (right) part of the figure shows the decomposition for atoms of sublattice A (B). The field is antiparallel to the  $z$  axis and leads to the magnon state assigned to sublattice A. For magnons of type B the direction of field  $\mathbf{h}$  is opposite.

in external field  $\mathbf{h}$  takes the form

$$\hat{\mathbf{H}} \begin{pmatrix} \psi_+ \\ \psi_- \end{pmatrix} = E \begin{pmatrix} \psi_+ \\ \psi_- \end{pmatrix} \quad (5)$$

with Hamiltonian

$$\hat{\mathbf{H}} = \hat{\mathbf{T}} \begin{pmatrix} 1 & 0 \\ 0 & 1 \end{pmatrix} + \sum_{n\nu} \mathbf{U}^+(\theta_\nu, \phi_{n\nu}) \mathbf{V}_\nu(\mathbf{r}_{n\nu}) \mathbf{U}(\theta_{n\nu}, \phi_{n\nu}) + h\sigma_z \quad (6)$$

where  $\hat{\mathbf{T}}$  is the operator of kinetic energy,  $n$  numbers unit cells,  $\nu$  numbers atomic sublattices,  $\mathbf{V}_\nu$  is two by two potential of the  $\nu$ th atom in the local atomic spin coordinate system,  $\mathbf{r}_{n\nu} = \mathbf{r} - \mathbf{a}_\nu - \mathbf{R}_n$ ,  $\mathbf{a}_\nu$  gives the position of the  $\nu$ th atom in the unit cell, angles  $\theta_\nu$  and  $\phi_{n\nu}$  specify the direction of the moment of the  $n\nu$ th atom,  $\phi_{n\nu} = \phi_\nu + \mathbf{q}\mathbf{R}_n$ ,  $\mathbf{U}(\theta_{n\nu}, \phi_{n\nu})$  is the standard spin- $\frac{1}{2}$  rotation matrix, and  $\sigma_z$  is the Pauli matrix. The action of the generalized translation on the spinor wave function

$$\Psi(\mathbf{r}) = \begin{pmatrix} \psi_+(\mathbf{r}) \\ \psi_-(\mathbf{r}) \end{pmatrix} \text{ has the form}$$

$$\{\alpha_{\mathbf{q}n} | E | \mathbf{R}_n \} \Psi(\mathbf{r}) = \mathbf{U}(\alpha_{\mathbf{q}n}) \Psi(\mathbf{r} - \mathbf{R}_n). \quad (7)$$

The Hamiltonian of a  $\mathbf{q}$ -magnon [Eq. (6)] commutes with generalized translations corresponding to given  $\mathbf{q}$ <sup>37,38</sup>. The symmetry properties of the Hamiltonian govern the symmetry properties of the calculated electron states that leads to the reproduction of the generalized translational symmetry of the Kohn-Sham Hamiltonian during iterations. Because of this, the fulfillment of the symmetry constraint [Eq. (4)] does not require application of a constraining field.

The symmetry with respect to the generalized translations fulfills the conditions of the generalized Bloch theorem and allows an exact reduction of the calculation

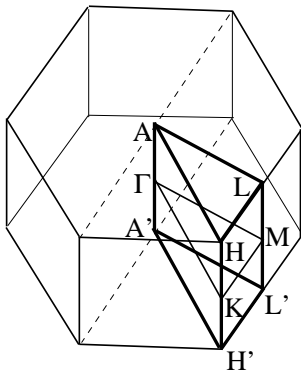


FIG. 4: Brillouin zone and irreducible domain for calculation of both electronic band structure of the AFM GS in the  $\mathbf{k}$  space and spin waves in the  $\mathbf{q}$  space.

for the spiral structure with arbitrary wave vector to the consideration of the small crystallographic unit cell of the crystal<sup>37</sup>.

### III. CALCULATION DETAILS

The calculations were performed with the augmented spherical waves (ASW) method<sup>39,40</sup>. The local density approximation (LDA) to the exchange-correlation functional is used<sup>41</sup>. The account for generalized translation symmetry and external magnetic field have been implemented earlier<sup>42,43</sup>. Therefore, only limited adaptation of the code were needed. In some of the calculations we used the LDA+ $U$  approach in the flavor of Dudarev et al.<sup>44</sup>.

The calculations were performed with three different  $\mathbf{k}$  meshes in the Brillouin zone (BZ) of the material (Fig. 4):  $n \times n \times n$ ,  $n=10, 20$ , and  $30$ . Here  $n$  is the number of the intervals in which the primitive vectors of the reciprocal lattice were divided. The results of the calculations have shown that the difference between spin wave energies obtained with  $n=20$  and  $n=30$  is usually small and most of the calculations reported in the paper were performed with  $n=20$ .

As mentioned above, a straightforward application of Eq. (1) assumes the existence of an interval of  $\Delta m_z$  where energy increase  $\Delta E$  is proportional to magnetization change  $\Delta m_z$ . Our calculations confirmed that usually such a linear dependence exists up to rather large deviation angles of the Mn atomic moments from the magnetization axis. Figure 5 shows typical characters of the dependences between calculated quantities and demonstrates high stability of the calculated magnon energy with respect to the value of the deviation of the Mn moments from the magnetization axis. The results of the calculations presented in the figure were obtained for wave vector  $\mathbf{q}=(0,0,0.3)$ . Here and in the rest of the paper we give the  $x$  and  $y$  components of the reciprocal space vectors in units of  $\frac{2\pi}{a}$  and the  $z$  components

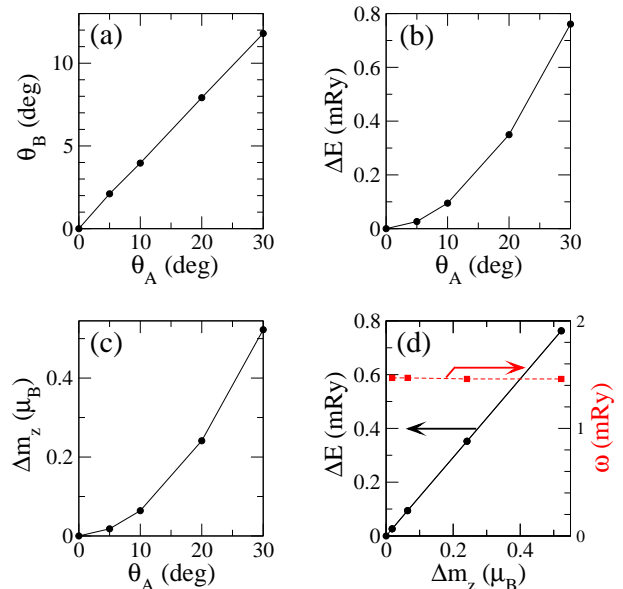


FIG. 5: The dependence of  $\Delta E$  on  $\Delta m_z$ . Figure shows calculations performed for magnon with wave vector  $\mathbf{q}=(0,0,0.3)$ . (a)-(c) The dependences of, respectively,  $\theta_B$ ,  $\Delta E$ , and  $\Delta m_z$  on  $\theta_A$ . (d) The dependence of energy increase  $\Delta E$  (black circles, left energy scala) and magnon energy  $\omega$  (red squares, right energy scala) on  $\Delta m_z$ .

in units of  $\frac{2\pi}{c}$ . We calculated constraining field  $h$  stabilizing the deviations of the Mn moments of sublattice A at following values:  $\theta_A=5^\circ, 10^\circ, 20^\circ, 30^\circ$ . Figure 5(a) gives calculated deviations of the moments of sublattice B,  $\theta_B$ . Figure (b) shows corresponding increase in energy  $\Delta E$ . The difference between  $\theta_A$  and  $\theta_B$  is the source of the magnetization change  $\Delta m_z$  shown in figure (c). In figure (d) we present the dependence of  $\Delta E$  on  $\Delta m_z$  which is very close to a linear one. The ratio of these quantities giving the magnon energy is with a good accuracy independent of  $\Delta m_z$ . In most of the calculations presented in the paper we used  $\theta_A=20^\circ$ . On the other hand, in the course of LDA+ $U$  calculations we dealt with the cases where strong deviation from the simple dependence of  $\Delta E$  on the deviation angle of the Mn atomic moments has been obtained showing the capacity of the method to reveal an instability in the studied system connected with the deviation of the atomic moments from the magnetization axis. These results are discussed in Sec. IV G.

## IV. SYMMETRY ASPECTS AND RESULTS OF CALCULATIONS

### A. SSG groups

The standard tool for the analysis of the symmetry properties of the crystalline materials is the apparatus of space groups. For magnetic systems an antisymmetry operation is included into consideration making extension

from space groups to magnetic space groups<sup>45</sup>. The antisymmetry operation that in an abstract treatment can be considered as changing the color between black and white in the magnetic case is responsible for the reversal of the magnetization. However, in the problems where the influence of the SOC can be neglected this tool is not sufficient for the description of the properties of magnetic systems. In particular, these limitations have been revealed for both electron band structure calculations and the studies based on the Heisenberg Hamiltonian of interacting atomic moments.

The solution of the problem has been found in the concept of SSG whose elements allow different transformation of the spin and space variables (see, e.g., Refs. 46–48). In recent years the interest to SSG has been revived. Reference 49 reports a detailed analysis of the magnon band topology within the framework of the Heisenberg and Heisenberg-Kitaev models of interacting atomic moments. Very recently several systematic works<sup>50–52</sup> were published devoted to the classification, properties, and applications of the SSGs.

The action of the SSG operator  $\{\alpha_S|\alpha_R|\boldsymbol{\tau}\}$  on the magnetization  $\mathbf{m}(\mathbf{r})$  is defined as

$$\{\alpha_S|\alpha_R|\boldsymbol{\tau}\}\mathbf{m}(\mathbf{r}) = \alpha_S\mathbf{m}([\alpha_R|\boldsymbol{\tau}]^{-1}\mathbf{r}) \quad (8)$$

where  $\alpha_S$  and  $\alpha_R$  are spin and space rotations respectively,  $\boldsymbol{\tau}$  is space translation, and we introduced notation  $[\alpha_R|\boldsymbol{\tau}] \equiv \{E|\alpha_R|\boldsymbol{\tau}\}$ . The action of the SSG operator on the two-component spinor has the form

$$\{\alpha_S|\alpha_R|\boldsymbol{\tau}\}\Psi(\mathbf{r}) = \mathbf{U}(\alpha_S)\Psi([\alpha_R|\boldsymbol{\tau}]^{-1}\mathbf{r}) \quad (9)$$

The generalized translations [Eq. (7)], crucial for the study of spiral magnetic configurations, are the operations of the SSG. The operation of time reversal acting on two-component spinor takes the form

$$\Theta = -i\sigma_y K = \begin{pmatrix} 0 & -1 \\ 1 & 0 \end{pmatrix} K \quad (10)$$

where  $K$  is the operator of complex conjugation. Since  $\begin{pmatrix} 0 & -1 \\ 1 & 0 \end{pmatrix}$  belongs to the set of unitary matrices  $\mathbf{U}$  entering Eq. (9), it already belongs to the SSG as an operation providing a spin rotation. Therefore, the complex conjugation  $K$  is also an allowed SSG operation. This means that the real form of the Kohn-Sham equations of collinear magnets [Eq. (6)] and its consequences become within SSGs a part of a straightforward symmetry treatment.

The success of the application of SSG compared with the application of space groups can be characterized as follows. The neglect of the SOC leads effectively to the replacement of the actual physical 3D space by the 6D space where spin and orbital variables are independent and can be transformed separately. The account for this freedom gives important new information about the properties of the system. In addition, the SSGs allow

a straightforward establishment of continuity relations between theoretical results obtained within different approximations, such as with and without SOC, or between the results obtained for collinear and helical magnetic configurations. The reason for this is the property that the SSG of the less symmetric case is the subgroup of the SSG of the more symmetric case. The latter feature plays important role in Sec. IV H where we discuss the transformation path of the electron band structure of a collinear magnet to the electron band structure of a magnon with a given wave vector  $\mathbf{q}$ .

Summarizing the applications in the paper of the symmetry concepts, we distinguish three different problems. The first was considered in Sec. II and uses the generalized translations as a symmetry constraint in the calculation of the magnon states. The second and third are, respectively, the altermagnetic spin-splitting of the electron states and chirality splitting of the magnon states.

## B. Degeneracy of the electron states in collinear magnets

The electronic band structure of collinear magnets has been calculated already for distinctly more than 50 years (see, e.g., Refs. 54,55). The electron wave functions were treated as scalar functions labeled with an index specifying the sign of the spin projection on the selected quantization axis. Respectively, two scalar Schrödinger equations were considered, one for each spin projection. The symmetry-caused degeneracy of the electron states arises in the following way. If  $g = [\alpha_R|\boldsymbol{\tau}]$  is a symmetry operation commuting with a scalar Schrödinger equation, the action of this operation on an eigenstate  $\psi_{\mathbf{k}\sigma}$  gives the eigenstate with the same energy, the same spin projection  $\sigma$ , and wave vector  $\alpha_R\mathbf{k}$ . The real form of the equation additionally gives the degeneracy of the electron states at points  $\mathbf{k}$  and  $-\mathbf{k}$ . The different vectors from the list of all  $\alpha_R\mathbf{k}$  and  $-\alpha_R\mathbf{k}$  vectors form the star  $\{\mathbf{k}\}$  of vector  $\mathbf{k}$ <sup>56</sup>.

In a FM, the Schrödinger equations for opposite spin projections are essentially different and, therefore, there is no symmetry-caused degeneracy of the spin-up and spin-down states. The spin splitting is the term characterizing this property of the electron structure which is valid for each point of the  $\mathbf{k}$  space.

On the other hand, in an AFM there must be degeneracy between the states with opposite spin projections. This degeneracy is the reason for the zero net magnetization of the AFM. To expose the origin of the spin degeneracy we first notice that in the Schrödinger equation for electrons with a given spin projection  $\sigma$  the electrons see different potentials at the atoms of different magnetic sublattices. Therefore at the first step only the operations leaving the sublattices invariant are considered. For each vector  $\mathbf{k}$  they give star  $\{\mathbf{k}\}_{subl}$  corresponding to the symmetry group of the sublattices. Next it is necessary to specify the symmetry operation that transforms

the equations corresponding to different spin projections into each other. The real-space part of this operation  $[\alpha_R^{tr}|\boldsymbol{\tau}]$  must transform the sublattices into each other and be accompanied by an 'antisymmetry' operation  $E'$  reversing the signs of the spin indices. As a consequence of such symmetry operation any spin-up state at point  $\mathbf{k}$  is degenerate with a spin-down state at  $\alpha_R^{tr}\mathbf{k}$ . This makes the system as a whole spin-compensated. The answer to the question whether the spin compensation takes place at each  $\mathbf{k}$  point of the BZ or only between different  $\mathbf{k}$  points depends on the properties of operation  $[\alpha_R^{tr}|\boldsymbol{\tau}]$  transforming the sublattices into each other. If vector  $\alpha_R^{tr}\mathbf{k}$  belongs to star  $\{\mathbf{k}\}_{subl}$  the degeneracy takes place at each  $\mathbf{k}\in\{\mathbf{k}\}_{subl}$ . In the opposite case we deal with an altermagnet with spin splitting at all points of the star  $\{\mathbf{k}\}_{subl}$ .

This approach to the symmetry properties of AFMs allows to reach the description of the electron structure without reference to the SSG. Its application to MnTe was reported in old publication Ref. 57. A very detailed and complete discussion of the application of this type of approach to the altermagnets was recently published by Turek<sup>58</sup>. This approach has shortcomings: Instead of treating the electron wave functions as spinors it considers them as scalars labeled with a spin index. This complicates the consideration of the influence on the electron band structure of the SOC or of the noncollinearity of the magnetic configuration where the account for spinor form of the electron wave functions is essential. Therefore, this approach is not sufficient for the purposes of this paper

where noncollinear incommensurate spiral structures are in the focus of the consideration.

The application of the SSG to the symmetry analysis of the collinear magnetic structures gives additional useful features. First, any spin rotation  $\{C_{z\phi}|E|0\}$  about the  $z$  axis is a symmetry operation of the spinor Kohn-Sham equation [Eqs. (5),(6)]. As the consequence of this symmetry the electron eigenfunctions assume one of the two spinor forms  $\psi(\mathbf{r})\begin{pmatrix} 1 \\ 0 \end{pmatrix}$  or  $\psi(\mathbf{r})\begin{pmatrix} 0 \\ 1 \end{pmatrix}$  corresponding to different irreducible representations (IR) of the SSG group<sup>59</sup>. Therefore, the spin-indexing of the electron functions is now a straightforward consequence of the symmetry of the problem and not the property imposed on the basis of additional arguments. Another consequence of the description of the collinear magnetic states in terms of SSG is that these states can be treated as spiral structures with arbitrary wave vectors  $\mathbf{q}$  and deviation angles  $\theta=0$ . Indeed, the group of generalized translations  $\mathbf{T}_{\mathbf{q}}$  with any  $\mathbf{q}$  is a subgroup of the group  $\mathbf{C}_z \times \mathbf{T}$  where  $\mathbf{T}$  is the group of space translations  $[E|\mathbf{R}_n]$  and  $\mathbf{C}_z$  is the group of all spin rotations  $C_{z\phi}$  about the  $z$  axis. This property will be used in Sec. IV H to study the transformation path of the electron structure of the collinear ground state into the electron structure of the magnon state with a given wave vector.

### C. Collinear AFM ground state of MnTe

In MnTe, the space group of the atomic lattice contains 24 point operations listed in Table I: 12 operations of type I transform the Mn sublattices into themselves whereas other 12 operations of type II transform them into each other. In the AFM state, the point operations of type II remain the part of the symmetry operations in combination with spin-index reversal operation.

The application of the 12 operations of type I to a reciprocal-space vector  $\mathbf{k}=(k_x, k_y, k_z)$  gives the set of 12 vectors with coordinates transformed according to the three columns of Table I with common heading  $\alpha_R\mathbf{r}$  or  $I\alpha_R\mathbf{r}$ . For instance, for the operation number 4 the transformed vector is  $(-\frac{1}{2}k_x - \frac{\sqrt{3}}{2}k_y, \frac{\sqrt{3}}{2}k_x - \frac{1}{2}k_y, k_z)$ . These 12 vectors are not necessarily different. For the most symmetric  $\Gamma$  point  $\mathbf{k}=(0,0,0)$  all vectors are equal and the corresponding star  $\{\mathbf{k}\}_{subl}$  consists of one vector. On the other hand, for a general point  $\mathbf{k}$  all 12 vectors are different. In Fig. 6 the points of the star  $\{\mathbf{k}\}_{subl}$  are shown for a general vector  $\mathbf{k}_o=(k_{ox}, k_{oy}, k_{oz})$  and marked as black circles: 6 points lie in the  $k_z=k_{oz}$  plane and other 6 points in the  $k_z=-k_{oz}$  plane. At 12 points of the star  $\{\mathbf{k}\}_{subl}$  thus obtained, for each electron state at point  $\mathbf{k}_o$  there are equivalent states with the same energy and the same spin projection.

As a representative of the operations of type II we will use the reflection in the  $xy$  plane (operation number 18 in Table I). Action with this operation on the vectors of the star  $\{\mathbf{k}_o\}_{subl}$  gives another 12 vectors shown in Fig. 6 as red squares. They differ from the vectors of the star  $\{\mathbf{k}_o\}_{subl}$  by the sign of the  $z$  component. The states at these 12 vectors are degenerate with the states at  $\mathbf{k}_o$  but have opposite spin projection. All 24 vectors are different and form full star  $\{\mathbf{k}_o\}$  of vector  $\mathbf{k}_o$ .

In general, for any  $\mathbf{k}$  we have the star  $\{\mathbf{k}\}_{subl}$  obtained with operation leaving magnetic sublattices invariant and the full star  $\{\mathbf{k}\}$  obtained with account for all symmetry operations. These two sets of vectors are either identical or the number of vectors in  $\{\mathbf{k}\}$  is double. In the former case, the change of the sign of the  $z$  component of the vectors from  $\{\mathbf{k}\}_{subl}$  does not change the set of vectors and at all points of the set there is spin degeneracy of the electron states whereas in the latter case at all points in  $\{\mathbf{k}\}$  there is the altermagnetic spin splitting.

The irreducible domain of the AFM MnTe is the triangular prism  $\Gamma\text{MKALH}$  that is  $\frac{1}{24}$ th of the BZ (Fig. 4). The analysis of all points of the irreducible domain shows that the altermagnetic spin splitting takes place at all inner points of the prism and, additionally, at inner points

TABLE I: Point symmetry elements. The following notations are used:  $E$  is the unity transformation,  $I$  is the space inversion,  $C_n^m$  is the rotation by angle  $2\pi\frac{m}{n}$ . In the column 'axis' the unit vectors parallel to the rotation axes are given. The two operations presented in each row have the same rotation axes. Columns headed  $\alpha_{RR}$  and  $I\alpha_{RR}$  give the coordinates of the vectors obtained after rotation of vector  $\mathbf{r} = (x, y, z)$ . In columns headed  $\tau$ , symbol  $\checkmark$  marks the symmetry operations containing non-primitive translation  $\tau=(0,0,0.5)$ . In the columns headed 'subl', the operations transforming the Mn sublattices into themselves are marked with  $\checkmark$ . For all direct-space vectors, the  $x$  and  $y$  coordinates are given in units of lattice parameter  $a$  and the  $z$  coordinate in units of lattice parameter  $c$ .

$N$	$\alpha_R$	axis	$\alpha_{RR}$			$\tau$	subl	$N$	$I\alpha_R$	$I\alpha_{RR}$			$\tau$	subl
1	$E$		$x$	$y$	$z$	-	$\checkmark$	13	$I$	$-x$	$-y$	$-z$	-	$\checkmark$
2	$C_6^1$	(0, 0, 1)	$\frac{1}{2}x - \frac{\sqrt{3}}{2}y$	$\frac{\sqrt{3}}{2}x + \frac{1}{2}y$	$z$	$\checkmark$	-	14	$IC_6^1$	$-\frac{1}{2}x + \frac{\sqrt{3}}{2}y$	$-\frac{\sqrt{3}}{2}x - \frac{1}{2}y$	$-z$	$\checkmark$	-
3	$C_6^5$	(0, 0, 1)	$\frac{1}{2}x + \frac{\sqrt{3}}{2}y$	$-\frac{\sqrt{3}}{2}x + \frac{1}{2}y$	$z$	$\checkmark$	-	15	$IC_6^5$	$-\frac{1}{2}x - \frac{\sqrt{3}}{2}y$	$\frac{\sqrt{3}}{2}x - \frac{1}{2}y$	$-z$	$\checkmark$	-
4	$C_6^2$	(0, 0, 1)	$-\frac{1}{2}x - \frac{\sqrt{3}}{2}y$	$\frac{\sqrt{3}}{2}x - \frac{1}{2}y$	$z$	-	$\checkmark$	16	$IC_6^2$	$\frac{1}{2}x + \frac{\sqrt{3}}{2}y$	$-\frac{\sqrt{3}}{2}x + \frac{1}{2}y$	$-z$	-	$\checkmark$
5	$C_6^4$	(0, 0, 1)	$-\frac{1}{2}x + \frac{\sqrt{3}}{2}y$	$-\frac{\sqrt{3}}{2}x - \frac{1}{2}y$	$z$	-	$\checkmark$	17	$IC_6^4$	$\frac{1}{2}x - \frac{\sqrt{3}}{2}y$	$\frac{\sqrt{3}}{2}x + \frac{1}{2}y$	$z$	-	$\checkmark$
6	$C_6^3$	(0, 0, 1)	$-x$	$-y$	$z$	$\checkmark$	-	18	$IC_6^3$	$x$	$y$	$-z$	$\checkmark$	-
7	$C_2$	(1, 0, 0)	$x$	$-y$	$-z$	-	$\checkmark$	19	$IC_2$	$-x$	$y$	$z$	-	$\checkmark$
8	$C_2$	$(\frac{1}{2}, \frac{\sqrt{3}}{2}, 0)$	$-\frac{1}{2}x + \frac{\sqrt{3}}{2}y$	$\frac{\sqrt{3}}{2}x + \frac{1}{2}y$	$-z$	-	$\checkmark$	20	$IC_2$	$\frac{1}{2}x - \frac{\sqrt{3}}{2}y$	$-\frac{\sqrt{3}}{2}x - \frac{1}{2}y$	$z$	-	$\checkmark$
9	$C_2$	$(-\frac{1}{2}, \frac{\sqrt{3}}{2}, 0)$	$-\frac{1}{2}x - \frac{\sqrt{3}}{2}y$	$-\frac{\sqrt{3}}{2}x + \frac{1}{2}y$	$-z$	-	$\checkmark$	21	$IC_2$	$\frac{1}{2}x + \frac{\sqrt{3}}{2}y$	$\frac{\sqrt{3}}{2}x - \frac{1}{2}y$	$z$	-	$\checkmark$
10	$C_2$	$(\frac{\sqrt{3}}{2}, \frac{1}{2}, 0)$	$\frac{1}{2}x + \frac{\sqrt{3}}{2}y$	$\frac{\sqrt{3}}{2}x - \frac{1}{2}y$	$-z$	$\checkmark$	-	22	$IC_2$	$-\frac{1}{2}x - \frac{\sqrt{3}}{2}y$	$-\frac{\sqrt{3}}{2}x + \frac{1}{2}y$	$z$	$\checkmark$	-
11	$C_2$	(0, 1, 0)	$-x$	$y$	$-z$	$\checkmark$	-	23	$IC_2$	$x$	$-y$	$z$	$\checkmark$	-
12	$C_2$	$(-\frac{\sqrt{3}}{2}, \frac{1}{2}, 0)$	$\frac{1}{2}x - \frac{\sqrt{3}}{2}y$	$-\frac{\sqrt{3}}{2}x - \frac{1}{2}y$	$-z$	$\checkmark$	-	24	$IC_2$	$-\frac{1}{2}x + \frac{\sqrt{3}}{2}y$	$\frac{\sqrt{3}}{2}x + \frac{1}{2}y$	$z$	$\checkmark$	-

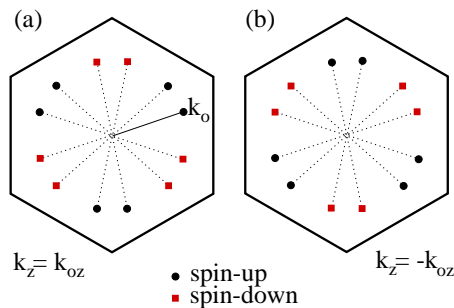


FIG. 6: Star  $\{\mathbf{k}_o\}$  of a general wave vector  $\mathbf{k}_o$ . The star contains 24 points lying in two planes  $k_z = k_{oz}$  [panel (a)] and  $k_z = -k_{oz}$  [panel (b)]. For any electron state at  $\mathbf{k}_o$ , the points shown by black circles contain equivalent states with the same spin projection. These 12 points form the star  $\{\mathbf{k}_o\}_{subl}$  corresponding to the symmetry group of the Mn sublattices. The points shown by red squares contain equivalent electron states with opposite spin projection. At all 24 points there is the altermagnetic spin splitting of the electron states. As discussed in Sec. IV E, the same figures reflect the properties of the chirality splitting of the magnons. In this case the wave vectors  $\mathbf{k}$  of the electron states must be replaced by corresponding magnon wave vectors  $\mathbf{q}$  and references to spin projections by references to chiralities.

of the face  $\Gamma$ MLA. At these points the calculations should be performed separately for the spin-up and spin-down states. Alternatively, the calculations can be performed in the  $\frac{1}{12}$ th of the BZ, prism ALHA'L'H' (Fig. 4), but for

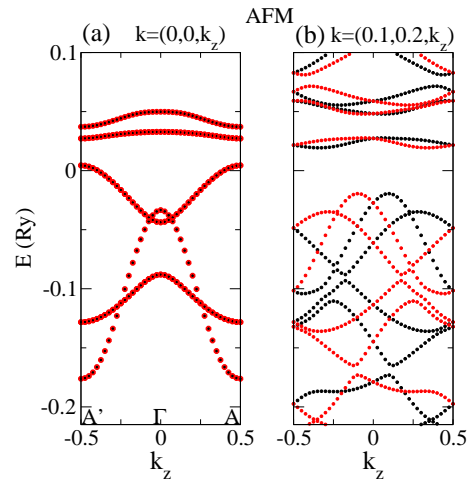


FIG. 7: Two fragments of the band structure of AFM MnTe. (a) High symmetry line  $(0,0,k_z)$  in the reciprocal space. (b) Low symmetry line  $(0.1,0.2,k_z)$  in the reciprocal space. Black (red) circles present spin-up (spin-down) states. At the points of the high symmetry line all states are spin degenerate. In the case of the low symmetry line there is altermagnetic spin splitting at all points with exception of the center and end points of the interval.

one spin projection only.

In Fig. 7 we show one fragment of the calculated band structure with spin-degenerate bands and one fragment with altermagnetic spin-splitting.



#### D. Magnetic structure of sublattices in magnon states

Let us discuss the properties of the structure of the AFM magnons that follow from the symmetry arguments. We consider the magnon with an arbitrary wave vector  $\mathbf{q}$ . The magnetic structure of the magnon is invariant with respect to the generalized translations corresponding to given  $\mathbf{q}$ . As stated above, the direct magnon

$$\mathbf{m}_{nA} = m_A \{ \sin(\theta_A) \cos[\mathbf{q}(\mathbf{a}_A + \mathbf{R}_n)], \sin(\theta_A) \sin[\mathbf{q}(\mathbf{a}_A + \mathbf{R}_n)], \cos(\theta_A) \} \quad (11)$$

$$\mathbf{m}_{nB} = m_B \{ \sin(\pi - \theta_B) \cos[\mathbf{q}(\mathbf{a}_B + \mathbf{R}_n) + \pi + \phi], \sin(\pi - \theta_B) \sin[\mathbf{q}(\mathbf{a}_B + \mathbf{R}_n) + \pi + \phi], -\cos(\theta_B) \}. \quad (12)$$

Because of the inequivalence of the sublattices it is expected that  $m_A \neq m_B$ ,  $\theta_A \neq \theta_B$ , and there is an unknown not symmetry-governed angle  $\phi$  specifying the phase shift between  $xy$ -projections of the moments of the two sublattices. The calculations with the suggested method confirmed that  $m_A \neq m_B$  and  $\theta_A \neq \theta_B$ . More details on these quantities will be given below.

However, concerning angle  $\phi$  the results of the calculations were unexpected: iterations started with an arbitrary selected  $\phi \neq 0$  resulted in the self-consistent magnetic configurations with  $\phi = 0$ . The question arises why the orientations of the moments of two inequivalent sublattices not connected by any symmetry operation are in such a strict coordination with each other. This type of the coordination is expected to be a symmetry-caused property. The explanation for this property is the following. The cone spiral structure of sublattice A [Eq. (11)] for arbitrary  $\mathbf{q}$  and  $\theta_A$  is invariant with respect to the SSG operation  $\{\Theta C_{2y} | I | 0\}$  that combines space inversion  $I$  and spin transformation  $\Theta C_{2y}$  performing spin reflection in the  $xz$  plane. This operation leaves invariant also the cone structure of the sublattice B [Eq. (12)] but only in the case of  $\phi = 0$  or  $\phi = \pi$ . This means that if the calculation is started with  $\phi = 0$  the value of  $\phi$  remains zero during iterations since the symmetry with respect to the operation  $\{\Theta C_{2y} | I | 0\}$  must be preserved. Thus, although there is no symmetry operation transforming the sublattices into each other there is an operation that is responsible for preserving  $\phi = 0$  and makes the two-sublattice magnetic configuration distinguished by an additional symmetry compared with the configurations obtained by a nonzero relative phase shift  $\phi$  between the sublattices. Hence, the choice of  $\phi = 0$  in the starting magnetic configuration imposes another symmetry constraint<sup>24</sup> in the magnon calculation that is additional to the constraint of generalized periodicity.

The presence of the 'hidden' symmetry operation effectively connecting inequivalent Mn sublattices influences also the properties of the Te atoms in the magnon states. In contrast to the Mn sublattices, the atoms of the two Te

calculation includes an effective magnetic field acting on both magnetic sublattices. This field is collinear to the  $z$  axis and therefore parallel to the magnetization of one sublattice and antiparallel to the magnetization of the other sublattice<sup>60</sup>. Hence the atoms of the two sublattices in the magnon state become inequivalent. On the basis of these conclusions, the magnetic configurations of the two sublattices in a magnon state can be written in the following form

sublattices remain equivalent because the space inversion transforms the Te sublattices into each other. This operation influences also the directions of the induced Te moments since to keep this symmetry operation intact the induced atomic moments of the two Te sublattices must transform into each other. The straightforward symmetry analysis gives for the Te atoms in the unit cell

$$\theta_C = \theta_D \equiv \theta_{Te} \neq 0 \quad (13)$$

$$\phi_C + \phi_D = \mathbf{q} \mathbf{R}_{IC} \quad (14)$$

where lattice vector  $\mathbf{R}_{IC} = \mathbf{a}_D - I \mathbf{a}_C$ . Although the values of angles  $\theta_C, \theta_D$  and  $\phi_C, \phi_D$  cannot be determined by symmetry arguments the knowledge of relations (13),(14) allows to accelerate the convergence process for the magnon configurations by adequate preparation of the initial magnetic configurations.

Here we give some further information concerning the calculated values of sublattice quantities entering Eqs. (11),(12). The values of the Mn moments appeared to be very robust and the difference between  $m_A$  and  $m_B$  was always small: for calculations with  $\theta_A = 20^\circ$  it never exceeded a few thousandth of Bohr magniton for estimated Mn atomic moments of  $\sim 4.2 \mu_B$ . On the other hand, the difference between  $\theta_A$  and  $\theta_B$  is an essential feature of the magnon states. It is strongly  $\mathbf{q}$ -dependent.

For field  $\mathbf{h}$  antiparallel to the  $z$  axis  $\theta_A > \theta_B$ . Such magnon states have negative magnetization with respect to the  $z$  axis and is associated with sublattice A. For field  $\mathbf{h}$  parallel to the  $z$  axis  $\theta_A < \theta_B$ , the magnetization is positive, and magnon is associated with sublattice B. The magnons associated with different sublattices have opposite chiralities.

For completeness we give some results of the calculation of the values and directions of the induced Te moments. The both characteristics are  $\mathbf{q}$  dependent. The induced moments deviate rather weakly from the  $z=0$  plane. For magnons of type A,  $\theta_{Te} > 90^\circ$  and the  $z$  component of the Te moments is negative. Respectively, for magnons of type B,  $\theta_{Te} < 90^\circ$  and the  $z$  component of

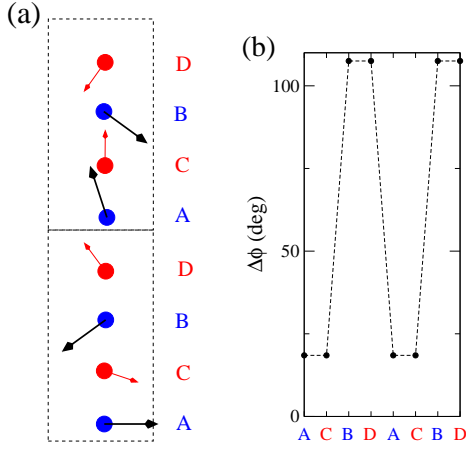


FIG. 8: (a) Directions of the projections of the atomic moments on the  $xy$  plane calculated for  $\mathbf{q}=(0,0,0.3)$  and  $\theta_A=20^\circ$ . The atomic labeling is according to Fig. 2. Two unit cells adjacent along the  $z$  axis are presented. (b) For each atom we show the value of the angle between the  $xy$  projection of its moment and of the moment of the atom lying next below.

the Te moments is positive. If the constrained deviation of the Mn moment is  $20^\circ$ , the maximal deviation of the Te moments from the  $z=0$  plane is about  $20^\circ$ . The values of the induced moments in this case do not exceed a few thousandth of Bohr magniton. Therefore the contribution of the Te moments to the magnetization of the magnon states that is collinear to the  $z$  axis is weak. On the other hand, the contribution of the induced moments into magnon energy can be noticeable. For chirality degenerate magnons of A and B type, the values of the Te moments and of their deviations from the  $z=0$  plane are exactly equal. For the chirality split magnons at a given  $\mathbf{q}$  the values are numerically different though in MnTe this difference is not large.

In Fig. 8(a) we show the directions of the projections of the moments on the  $xy$  plane calculated for  $\mathbf{q}=(0,0,0.3)$  and  $\theta_A=20^\circ$ . Two unit cells adjacent along the  $z$  axis are presented. The directions of the atomic moments in the second unit cell rotate by angle  $\mathbf{q}\mathbf{R}$  with respect to the corresponding moments in the first unit cell. Here  $\mathbf{R}$  is the lattice vector connecting the cells. The relative directions of the Mn moments of sublattices A and B in the same unit cell are also according to wave vector  $\mathbf{q}$ :  $\phi_B-\phi_A=\mathbf{q}(\mathbf{a}_B-\mathbf{a}_A)+\pi$  that is the consequence of  $\phi=0$  in Eq. (12). The directions of the Te moments (atoms C and D) within one unit cell cannot be uniquely determined by symmetry. There is, however, symmetry property of equal angles of the Te moments with respect to the moment of the Mn atom lying between them. On the other hand, these angles are different for the Mn atoms of the A and B sublattices reflecting their inequivalence in the magnon states. Figure 8(b) presents for each atom the value of the angle between the  $xy$  projection of its moment and of the moment of the atom lying next below. As seen in figure (a), this is always the angle between the

moments of the Mn and Te atoms. These angles are distinctly different for Mn atoms of the A and B sublattices confirming again their inequivalence.

### E. Chirality splitting of magnons in altermagnets

To study the chirality properties of magnons the approach to the symmetry analysis must be fundamentally revised compared to the spin-splitting study of the electron states discussed above (Sec. IV B). Now the analysis is focused not on the properties of the electron states of the same magnetic configuration but on the relation between energies of different magnetic configurations. If we take an arbitrary SSG operation  $\{\alpha_S|\alpha_R|\boldsymbol{\tau}\}$  and transform our magnetic system according Eq. (8) we obtain the system with the properties directly related to the properties of the initial system. This conservation of the properties reflects two factors: first, the homogeneity and anisotropy of the space where the system is placed and, second, the invariance under the applied transformation of the form of the interactions taken into account in the considered physical model<sup>61</sup>. In particular, the equivalence of the systems connected by the SSG transformation reflects the fact that both space shift and space rotation of the system does not change the energy of the system. To reveal the magnon states having, for symmetry reasons, equal energies we will act with operations  $\{\alpha_S|\alpha_R|\boldsymbol{\tau}\}$  on a selected magnon state aiming to determine other magnon states equivalent to it. Since dealing with the magnon states of the system we are not interested in the copies of the system obtained by the displacement of the atomic lattice or by the rotation of the net sublattice magnetization from the  $z$  axis the operations we consider are restricted to follows: the orbital part  $[\alpha_R|\boldsymbol{\tau}]$  of the transformation belongs to the space group of the crystal and leaves the lattice unchanged whereas the spin transformation  $\alpha_S$  keeps the net magnetizations of the sublattices collinear to the  $z$  axis.

If  $[\alpha_R|\boldsymbol{\tau}]$  transforms magnetic sublattices into themselves the spin part must keep the directions of the sublattice magnetizations unchanged  $\alpha_S\mathbf{e}_z=\mathbf{e}_z$ . Here  $\mathbf{e}_z$  is the unity vector parallel to the  $z$  axis. Respectively, if  $[\alpha_R|\boldsymbol{\tau}]$  transforms sublattices into each other the spin part must reverse the directions of the sublattice magnetizations  $\alpha_S\mathbf{e}_z=-\mathbf{e}_z$ . This shows that the set of the operations we need to consider forms exactly the SSG of the collinear AFM ground state that is the group used above (Sec. IV B) in the discussion of the altermagnetic spin-splitting of the electronic states of the GS collinear configuration.

This conclusion reveals a direct analogy between the pattern of the spin-splitting of the electron states in the  $\mathbf{k}$  space and the pattern of the chirality splitting of the spin waves in the  $\mathbf{q}$  space. Indeed, if  $\alpha_R$  transforms  $\mathbf{k}$  vector of an electron state in  $\alpha_R\mathbf{k}$  it transforms  $\mathbf{q}$  vector of a magnon in  $\alpha_R\mathbf{q}$ . And if this operation reverses spin of the electron state it changes also the chirality of the magnon.

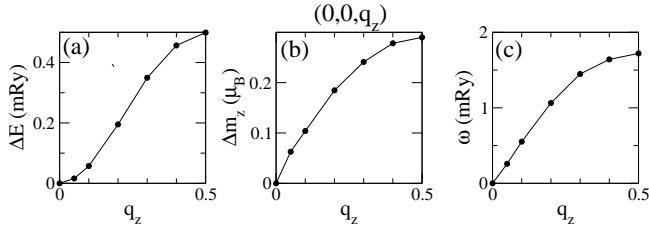


FIG. 9: Calculation of the spin wave energies in the  $\Gamma A$  interval of the BZ:  $\mathbf{q}=(0,0,q_z)$ ,  $q_z \in [0,0.5]$ . (a)  $\Delta E$ , (b)  $\Delta m_z$ , (c) spin wave energy  $\omega$ .

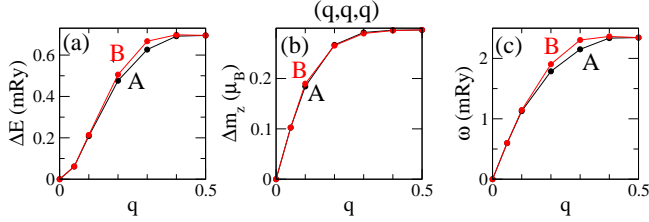


FIG. 10: Calculation of the spin wave energies in the interval  $\mathbf{q}=(q,q,q)$ ,  $q \in [0,0.5]$ . (a)  $\Delta E$ , (b)  $\Delta m_z$ , (c) spin wave energy  $\omega$ . Black curves show the results for magnons of type A, red curves for magnons of type B.

Hence if there is spin-splitting (spin-degeneracy) of the electron states at point  $\mathbf{k}$  there is also the chirality splitting (chirality degeneracy) of the magnon states for wave vector  $\mathbf{q}=\mathbf{k}$ . Therefore the reciprocal-space symmetry patterns of the spin splitting in the ground state electron band structure and chirality splitting of magnons are identical. In particular, Fig. 6 reflecting spin splitting of the electron states in the  $\mathbf{k}$  space is directly applicable to the analysis of the chirality splitting of the magnons in the  $\mathbf{q}$  space.

#### F. Calculated magnon dispersion

In Fig. 9 we show the results of the calculation of the spin wave energies in the  $\Gamma A$  interval of the BZ:  $\mathbf{q}=(0,0,q_z)$ ,  $q_z \in [0,0.5]$ . Close to the  $\Gamma$  point the energy increase  $\Delta E \sim q_z^2$  whereas  $\Delta m_z \sim q_z$ . This gives a linear dependence of the spin wave energy  $\omega$  on  $q_z$ , as expected for the magnons in AFMs in the region of the  $\Gamma$  point. In agreement with symmetry arguments, the magnons of both chiralities are degenerate at the wave vectors from this interval.

From the symmetry analysis (Sec. IVE) it is expected that for the wave vectors lying on a less symmetric line we should obtain chirality splitting of the magnon states. In Fig. 10 we show the result of the calculations for interval  $\mathbf{q}=(q,q,q)$ ,  $q \in [0,0.5]$ . The calculations confirm the prediction of the symmetry analysis: numerical difference between data for A and B magnons is obtained for all points of the interval with exception for the end points. However, the difference is small and, for a part of the

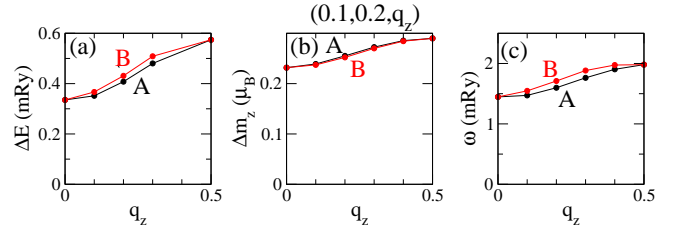


FIG. 11: Spin wave energies in the interval  $\mathbf{q}=(0.1,0.2,q_z)$ ,  $q_z \in [0,0.5]$ . (a)  $\Delta E$ , (b)  $\Delta m_z$ , (c) spin wave energy  $\omega$ . Black curves show the results for magnons of type A, red curves for magnons of type B.

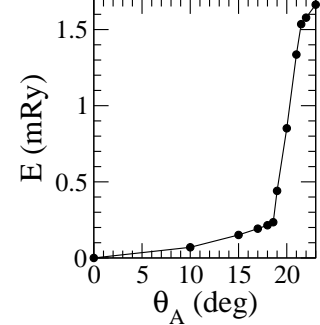


FIG. 12: Instability of the energy of magnon state with respect to the number of magnons.

interval, is not noticeable in the figure.

In Fig. 11 we show the result of the calculations for an interval  $\mathbf{q}=(0.1,0.2,q_z)$ ,  $q_z \in [0,0.5]$  in the reciprocal space. This interval contains general points not invariant with respect to any symmetry operation. Again the calculations confirm the results of the symmetry analysis: at all inner points of the interval there is chirality splitting of the magnon states. The maximal splitting is  $\sim 7\%$  with respect to the energy of the spin waves at the corresponding  $\mathbf{q}$  point.

#### G. Instability of the energy of magnon state with respect to the number of magnons

Studying the performance of the method in different situations we applied LDA+ $U$  method with various parameters. We noticed that in some cases there is a strong dependence of the magnon-state energy on the small variation of the parameters of the calculations such as the value of the constrained angle  $\theta$  or the value of Hubbard parameter  $U$ . Since the nonmagnetic atoms, in our case Te atoms, play crucial role in the formation of altermagnetism, the character of the hybridization of the electron states of magnetic and nonmagnetic atoms is decisive for the strength of the altermagnetic effects. To influence the position of the Te 5p states with respect to the Mn 3d states we used not only parameter  $U_{Mn}$  for the Mn 3d

states, usual for the LDA+ $U$  method, but also parameter  $U_{Te}$  for the Te 5p states. Parameter  $U_{Te}$  was treated as a free parameter of the model and was allowed to assume negative values. We emphasize that these model calculations were performed to investigate the potential of the method and we do not connect the results of the modeling with properties of the particular material.

In Fig.12, we show a typical instability behavior. This result was obtained for the energy of the magnon states of type A with wave vector  $\mathbf{q}=(0.1,0.2,0.3)$  calculated as a function of constrained angle  $\theta_A$  with parameters  $U_{Mn}=0.2$  Ry, and  $U_{Te}=-0.03$  Ry. The increase of  $\theta_A$  can be associated with increasing number of magnons. Around  $\theta_A$  of  $20^\circ$  the system experiences sharp transformation between two different states. It is straightforward to suppose that in this  $\theta_A$  region, the increase of  $\theta_A$  leads to the change of the relative energy positions of different groups of electron states in the band structure of the system. In the iterations, the consequences of this process are enhanced leading to the sharp variation of the energy of the magnon state.

A similar unstable behavior we obtained for magnon B as a function of the constrained angle  $\theta_B$  (not shown). However, the region of instability was shifted to somewhat smaller angles. As the result, in the instability region we obtained an enhancement of the chirality splitting effect. Thus, for  $\theta_A=\theta_B=20^\circ$  the difference in energies of the A and B magnon states is  $\sim 0.6$  mRy that is about two orders of value larger than for angles of  $15^\circ$ . Similar instability was obtained in calculations for other wave vectors  $\mathbf{q}$ . Also, this type of singular behavior was obtained for the magnon state energy as the function of parameter  $U_{Te}$  (not shown). In the latter calculations constrained angle  $\theta$  was fixed at  $20^\circ$ . The presence of such instabilities cannot be noticed applying the standard procedure of mapping on the Heisenberg Hamiltonian.

#### H. Relation between electronic band structures of the magnon states and chirality properties of these states

Both chirality splitting and chirality degeneracy of two magnons manifest certain relation between the energies of the magnons. Whether two magnons are equivalent and have equal energies or are inequivalent and have different energies must be reflected in the properties of their electron band structures. In this section we gain an insight into the connection between electronic band structures of the magnon states and chirality properties of these states.

The concepts of the generalized periodicity [Eq. (4)] and generalized Bloch theorem<sup>37</sup> will help us to establish the transformation path from the electronic band structure of the collinear AFM GS to the electronic band structure of the magnon with a given wave vector  $\mathbf{q}$  and given chirality. In this way we reveal the features of the electron energy spectrum connected with the presence or absence of the chirality splitting.

We begin with the electron band structure of the ground state. As pointed out in Sec. IV B, the collinear magnetic ground state can be treated as a spiral with  $\theta=0$  and arbitrary wave vector  $\mathbf{q}$ . Different  $\mathbf{q}$  values lead to different relative shifts of the spin-up and spin-down electron states in the reciprocal space. This shift is the consequence of the redefinition of the wave vector of the electron state in the case of the generalized Bloch theorem compared to the usual periodicity and usual Bloch theorem<sup>38</sup>: depending on spin projection  $\sigma$  wave vector of the electron state changes from  $\mathbf{k}$  to  $\mathbf{k}-\sigma\mathbf{q}/2$ . Since in the collinear AFM GS there is no mixing between spin-up and spin-down electron states the relative shift of these states in the reciprocal space has no consequences for physically significant characteristics. However, in the noncollinear magnon state with  $\theta\neq 0$ , the wave vector  $\mathbf{q}$  is uniquely defined. The relative shift by vector  $\mathbf{q}$  of the spin-up and spin-down states is the first step in the transformation of the band structure that brings the wave vectors of the electron states in agreement with the definition according to the generalized Bloch theorem, the only possible way to introduce the wave vector in the case of noncollinear spiral structures.

The detailed process of the transformation of the shifted GS electronic band structure to the electronic band structure of the magnon in a real multiple-band system is complex and can be obtained only numerically. However, some important general trends can be distinguished. One of the consequences of the noncollinearity is the hybridization of the spin-up and spin-down electron states. The strongest hybridization takes place in the regions of the intersection of the spin-up and spin-down bands. From the symmetry point of view, in the collinear ground state the spin-up and spin-down electron states belong to different IRs of the SSG group and the corresponding bands intersect. In the magnon state the number of the symmetry operations decreases and spin-up and spin-down states do not any longer belong to different IRs that leads to their hybridization. The hybridization leads to the repulsion of the bands at the intersection points.

We remark that besides the hybridization repulsion of the bands with opposite spin projections in the electron structure of the helical configuration the noncollinearity leads also to the transformation of the electron bands with a given spin projection that has the form of mixing of the  $\mathbf{k}-\mathbf{q}/2$  and  $\mathbf{k}+\mathbf{q}/2$  states of the GS electron structure with coefficients  $\cos^2\frac{\theta}{2}$  and  $\sin^2\frac{\theta}{2}$  (Ref. 37). This effect is quadratic with respect to  $\theta$  while the spin-mixing effect at the intersection point is linear in  $\theta$ .

Since the positions of the band intersections are different for different  $\mathbf{q}$ , the process of the hybridization is  $\mathbf{q}$  dependent and, therefore, different for different magnons. Let us look closer at the transformation of the band structure for two values of the magnon wave vector  $\mathbf{q}$ : high symmetry vector  $\mathbf{q}_1 = (0, 0, 0.2)$  and general vector  $\mathbf{q}_2 = (0.1, 0.2, 0.2)$ . On the basis of both the symmetry analysis and the calculations discussed in Secs. IV E, IV F

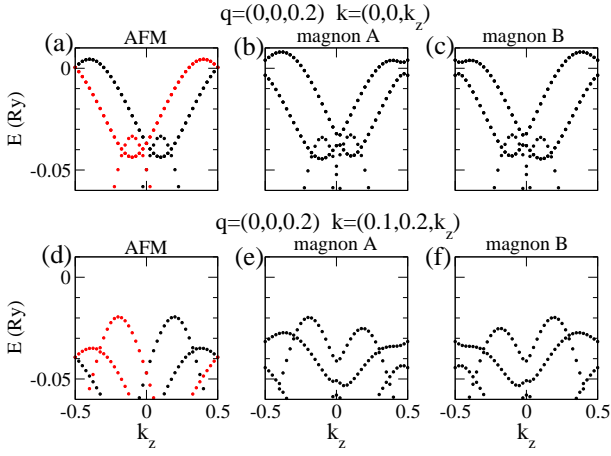


FIG. 13: The transformation of the electron band structure of the AFM GS to the band structure of magnon states with  $\mathbf{q}_1 = (0, 0, 0.2)$ . Figures (a)-(c) present the bands in the interval  $[0, 0, k_z]$ ,  $k_z \in [-0.5, 0.5]$  of the electron BZ. The usual AFM band structure in this interval is shown in Fig. 7(a). Figure (a) gives the AFM band structure after the shift of the bands by  $\frac{1}{2}\sigma\mathbf{q}_1$ . Figures (b) and (c) give the electron bands for magnon structures of the A and B types. Figures (d)-(f) give the band structure in the interval  $[0.1, 0.2, k_z]$ ,  $k_z \in [-0.5, 0.5]$ . Corresponding usual AFM band structure is shown in Fig. 7(b). Figure (d) gives the AFM band structure after the shift of the bands by  $\frac{1}{2}\sigma\mathbf{q}_1$ . Figures (e) and (f) give the electron bands for magnon structures of the A and B types. In Figs. (a) and (d), black (red) circles present spin-up (spin-down) states.

we know that at  $\mathbf{q}_1$  the magnons are chirality-degenerate whereas at  $\mathbf{q}_2$  they are chirality-split.

We begin with  $\mathbf{q}_1$  and consider electron band structure in the interval  $[0, 0, k_z]$ ,  $k_z \in [-0.5, 0.5]$ , in the  $\mathbf{k}$  space. On the high symmetry line  $(0, 0, k_z)$  the GS band structure is spin degenerate [Fig. 7(a)]. The relative shift by  $\mathbf{q}_1$  results in spin split bands as shown in Fig. 13(a). The change of the sign of  $k_z$  combined with the spin reversal leaves the band structure in Fig. 13(a) invariant. The band structures of magnon configurations of both chiralities calculated for wave vector  $\mathbf{q}_1$  and  $(0, 0, k_z)$  line are presented in Figs. 13(b),(c). For magnon configuration of type A we used angles  $\theta_A=45$  and  $\theta_B=0$ , for magnon of type B angles  $\theta_A=0$  and  $\theta_B=45$ . Since in noncollinear structures the electron states are spin-mixed, all states are shown in the same color. The band structures of magnons A and B are different and both of them have lost the symmetry with respect to the reflection at  $k_z=0$ . However, these band structures transform to each other after reflection at  $k_z=0$  and, therefore, the integrals over the occupied parts of the spectra for the given  $\mathbf{k}$  interval are equal for both magnons.

Let us continue with the consideration of a low symmetry interval  $[0.1, 0.2, k_z]$ ,  $k_z \in [-0.5, 0.5]$ . The bands have alternating spin splitting in the collinear AFM configuration [Fig. 7(b)]. There is the symmetry of the band structure with respect to simultaneous sign change of

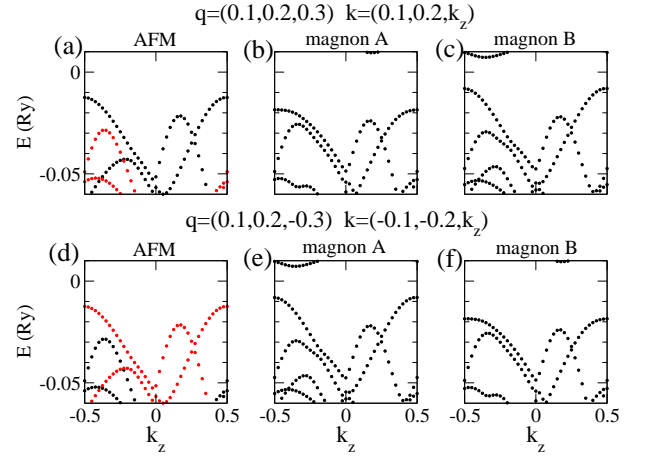


FIG. 14: The transformation of the electron band structure of the AFM GS to the band structures of magnon states with wave vectors  $\mathbf{q}_2 = (0.1, 0.2, 0.3)$  and  $\mathbf{q}_3 = (0.1, 0.2, -0.3)$ . Figures (a)-(c) give the band structures in the interval  $[0.1, 0.2, k_z]$ ,  $k_z \in [-0.5, 0.5]$  of the electron BZ for wave vector  $\mathbf{q}_2$ . Figure (a) presents the AFM bands after the shift by  $\frac{1}{2}\sigma\mathbf{q}_2$ . Figures (b) and (c) give the electron bands for magnon structures of the A and B type. Figures (d)-(f) show the band structures in the interval  $[-0.1, -0.2, k_z]$ ,  $k_z \in [-0.5, 0.5]$  for wave vector  $\mathbf{q}_3$ . Figure (d) gives the AFM bands after the shift by  $\frac{1}{2}\sigma\mathbf{q}_3$ . Figures (e) and (f) give the electron bands for magnon structures of the A and B type. In Figs. (a) and (d), black (red) circles present spin-up (spin-down) states.

both  $k_z$  and spin projection similar to the case shown in Fig. 13(a). After the shift by  $\frac{1}{2}\sigma\mathbf{q}_1$  [Fig. 13(d)] the symmetry between the spin-up and spin-down bands remains intact. The calculation for the A and B magnon configurations for this  $\mathbf{q}$  gives, similar to the  $(0, 0, k_z)$  interval, two different band structures [Fig. 13(e),(f)] which have lost the reflection symmetry. However, they again transform into each other after reflection at  $k_z = 0$ . Therefore, also in this case the integrals over occupied parts of the band structures of both magnons are identical. These symmetry properties provide an insight into why the magnons with opposite chiralities are degenerate at  $\mathbf{q}_1=(0,0,0.2)$ .

Now let us consider the magnons with low symmetry wave vector  $\mathbf{q}_2=(0.1,0.2,0.3)$  that is not invariant with respect to any space group transformation. We take again the  $[0.1, 0.2, k_z]$  interval of the BZ. After  $\frac{1}{2}\sigma\mathbf{q}_2$  shift in the GS band structure [Fig. 14(a)] we obtain in this interval the spin-up and spin-down bands that are essentially different and cannot be transformed into each other by a symmetry operation. Respectively, magnons A and B result in this case in two essentially different band structures [Figs. 14(b),(c)] giving different energy contributions to the integral band energies of the A and B magnons. The difference of the band structures of the A and B magnons with wave vector  $\mathbf{q}_2$  illustrates the origin of the chirality splitting of the magnons at this wave vector.

On the other hand, for  $\mathbf{q}_3=(0.1,0.2,-0.3)$  in the  $[-0.1,-0.2,k_z]$  interval we obtain the band structures [Figs. 14(d)-(f)] very similar to those shown in Figs. 14(a)-(c). Figure 14(d) for the AFM GS is identical to Fig. 14(a) after reversal of the spin projections of all electron states. The band structure of magnon A with wave vector  $\mathbf{q}_3$  [Fig. 14(e)] is identical to the band structure of magnon B with wave vector  $\mathbf{q}_2$  [ Fig. 14(c)]. The band structure of magnon B with wave vector  $\mathbf{q}_3$  [Fig. 14(f)] is identical to the band structure of magnon A with wave vector  $\mathbf{q}_2$  [ Fig. 14(b)]. These properties of the band structures illustrate the band-structure basis of the chirality degeneracy of the magnons with different wave vectors and chirality splitting at given wave vectors.

The following point is worth emphasizing: As noted above, in the band structures of magnons (Figs. 13,14) the electron states are spin mixed and, therefore, all bands are presented in the same color. However, the contributions of the spin-up and spin-down components of the spinor eigenfunctions are different for different states. Some of the electron states can remain almost spin-up or almost spin-down. On the other hand, in the regions where spin-up and spin-down bands intersect in the GS the hybridization leads to the electron states with large contributions of both spin projections. For magnons, the integrated spin contributions of the occupied electron states do not completely compensate each other since each magnon has a nonzero magnetic moment.

## V. CONCLUSIONS

In the paper we suggest the method for direct ab initio calculation of magnons in complex collinear magnets with weak influence of the spin-orbit coupling. The method does not include the mapping of the electron system on the Heisenberg Hamiltonian of the interacting atomic moments as an intermediate step.

Each magnon state is obtained in a separate DFT based self-consistent calculation performed under two different constraints. One constraint governs the magnetization change with respect to the ground state and the other is a symmetry constraint establishing the value of the magnon wave vector  $\mathbf{q}$ . The performance of the method is demonstrated by the application to an altermagnet MnTe. The main feature of the GS of the altermagnets is the spin splitting of the electron states with a given wave vector  $\mathbf{k}$ . Also the magnons in altermagnets have a special feature: chirality splitting of magnons with the same wave vector  $\mathbf{q}$  that is the energy difference of the magnons corresponding to the different magnetic sublattices. We show that despite different nature of the spin-splitting of the electron states and chirality splitting of the magnon states have identical patterns in the corresponding wave vector spaces. All conclusions based on the symmetry arguments are confirmed by the results of numerical calculations.

We investigate the connection between the chirality properties of the magnons and the properties of the electron band structures of the magnons. The deep connection between these two different energy characteristics is exposed.

The altermagnetism of MnTe is the consequence of the presence of the Te atoms. Therefore an adequate attention is devoted to the analysis of the selfconsistent response of the Te atoms in the magnon states. In particular, we show that the Te atoms remain equivalent in the magnon states though the Mn atoms belonging to different sublattices became inequivalent. The information about induced magnetic moments of the Te atoms obtained in the symmetry analysis helps to accelerate the convergence of the magnon states by means of optimizing the initial magnetic configuration.

In the paper, different symmetry aspects are analyzed within the framework of the spin space groups. These aspects include the symmetry constraint of generalized periodicity in the suggested method of the magnon calculations, the spin splitting of the electron states in the GS, and chirality splitting of the magnon states. The SSGs that are the generalization of the usual space groups allow the integration of these different aspects in one coherent physical picture.

The suggested method accompanied with symmetry arguments on the basis of the spin-space groups provides a new efficient tool for first principles study of the magnons in complex collinear magnets including emerging class of altermagnets.

The spin splitting in some of the AFM crystals was known for many years but only few years ago it became the focus of intense research efforts within the new research field dubbed altermagnetism. Possible applications of the altermagnetic spin splitting are under discussion. On the other hand, the chiral splitting of the magnon states that is a fundamental feature of altermagnets has been noticed very recently. Though important from the theoretical point of view, this splitting seems to be relatively weak. However, also this feature of altermagnets can become important for future experimental studies and practical applications in the field of magnonics. A necessary step on this path is the search for materials with large chirality splitting. Our method that self-consistently takes into account the crucial contribution of the nonmagnetic atoms provides a useful tool in this search. Also, the ability of the method to reveal possible chirality-sensitive instabilities of the magnon excitations can prove itself useful in this respect.

## VI. ACKNOWLEDGEMENTS

K.C. acknowledges financial support by Czech Science Foundation, grant no. 23-04746S. V.M.S. acknowledges financial support by grant PID2022-139230NB-I00 funded by MCIN/AEI/10.13039/501100011033.

- <sup>1</sup> B. Flebus et al., J. Phys.: Condens. Matter **36**, 363501 (2024).
- <sup>2</sup> A. V. Chumak et al., IEEE Transactions on Magnetics, **58**, 1 (2022).
- <sup>3</sup> A. Barman et al., J. Phys.: Condens. Matter **33**, 413001 (2021).
- <sup>4</sup> H. J. Qin, Kh. Zakeri, A. Ernst, L. M. Sandratskii, P. Buczek, A. Marmodoro, T. -H. Chuang, Y. Zhang, and J. Kirschner, Nat. Commun. **6**, 6126 (2015).
- <sup>5</sup> Ch. Kittel, *Introduction to Solid State Physics* (Wiley, 2004).
- <sup>6</sup> S. V. Halilov, H. Eschrig, A. Y. Perlov, and P. M. Oppeneer, Phys. Rev. B **58**, 293 (1998).
- <sup>7</sup> Q. Niu, Xindong Wang, L. Kleinman, and Wu-Ming Liu, D. M. C. Nicholson, and G. M. Stocks, Phys. Rev. Letters, **83**, 207 (1999).
- <sup>8</sup> S. Y. Savrasov, Phys. Rev. Lett., **81**, 12, 2570 (1998).
- <sup>9</sup> P. Buczek, A. Ernst, and L. M. Sandratskii, Phys. Rev. B **84**, 174418 (2011).
- <sup>10</sup> L. M. Sandratskii and P. Buczek, Phys. Rev. B **85**, 020406(R) (2012).
- <sup>11</sup> M.M. Odashima, A. Marmodoro, P. Buczek, A. Ernst, and L. Sandratskii, Phys. Rev. B **87**, 174420 (2013).
- <sup>12</sup> Samir Lounis, Manuel dos Santos Dias, and Benedikt Schweglinghaus, Phys. Rev. B **91**, 104420 (2015).
- <sup>13</sup> T. Skovhus and T. Olsen, Phys. Rev. B **103**, 245110 (2021).
- <sup>14</sup> X. Liu, L. Yihao, and J. Feng, Phys. Rev. B **108**, 094405 (2023).
- <sup>15</sup> A. I. Liechtenstein, M. I. Katsnelson, V. P. Antropov, and V. A. Gubanov, J. Magn. Magn. Mater. **67**, 65 (1987).
- <sup>16</sup> S. Mankovsky, and H. Ebert, Electron. Struct. **4**, 034004 (2022).
- <sup>17</sup> I. Turek, J. Kudrnovský, V. Drchal, and P. Bruno, Philosophical Magazine, **86**, 1713 (2006).
- <sup>18</sup> S. Mu, R. P. Hermann, S. Gorsse, H. Zhao, M. E. Manley, R. S. Fishman, and L. Lindsay, Phys. Rev. Materials **3**, 025403 (2019).
- <sup>19</sup> G. Martinez-Carracedo, L. Oroszlany, A. Garcia-Fuente, B. Nyari, L. Udvardi, L. Szunyogh, and J. Ferrer, Phys. Rev. B **108**, 214418 (2023).
- <sup>20</sup> M. Ležaić, Ph. Mavropoulos, J. Enkovaara, G. Bihlmayer, and S. Blügel, Phys. Rev. Lett. **97**, 026404 (2006).
- <sup>21</sup> L. M. Sandratskii, R. Singer, E. Sasioglu, Phys. Rev. B **76**, 184406 (2007).
- <sup>22</sup> J. Söderquist and T. Olsen, Appl. Phys. Lett. **124**, 182409 (2024).
- <sup>23</sup> Attila Szilva, Yaroslav Kvashnin, Evgeny A. Stepanov, Lars Nordström, Olle Eriksson, Alexander I. Lichtenstein, and Mikhail I. Katsnelson, Rev. Mod. Phys. **95**, 035004 (2023).
- <sup>24</sup> L. M. Sandratskii, Phys. Rev. B **64**, 134402 (2001).
- <sup>25</sup> L. Šmejkal, J. Sinova, and T. Jungwirth, Physical Review X **12**, 031042 (2022),
- <sup>26</sup> L. Šmejkal, J. Sinova, and T. Jungwirth, Phys. Rev. X **12**, 040501 (2022).
- <sup>27</sup> I. Mazin, Phys. Rev. X **12**, 040002 (2022).
- <sup>28</sup> L. Bai, W. Feng, S. Liu, L. Šmejkal, Y. Mokrousov, and Y. Yao, Advanced Functional Materials, 2409327 (2024).
- <sup>29</sup> S. Reimers et al., Nat. Commun. **15**, 2116 (2024).
- <sup>30</sup> J. Krempaský et al., Nature **626**, 517 (2024).
- <sup>31</sup> I. I. Mazin, Phys. Rev. B **107**, L100418 (2023).
- <sup>32</sup> O. Fedchenko et al., Sci. Adv. **10**, eadj4883 (2024).
- <sup>33</sup> L. Šmejkal, A. Marmodoro, Kyo-Hoon Ahn, R. González-Hernández, I. Turek, S. Mankovsky, H. Ebert, S. W. D'Souza, O. Šipr, J. Sinova, and T. Jungwirth, Phys. Rev. Lett. **131**, 256703 (2023).
- <sup>34</sup> Zheyuan Liu, Makoto Ozeki, Shinichiro Asai, Shinichi Itoh, and Takatsugu Masuda, Phys. Rev. Lett. **131**, 156702 (2024).
- <sup>35</sup> S. M. Rezende, A. Azevedo, and R. L. Rodríguez-Suárez, J. Appl. Phys. **126**, 151101 (2019).
- <sup>36</sup> L. M. Sandratskii, Adv. Phys. **47**, 91 (1998).
- <sup>37</sup> L. M. Sandratskii, phys. stat. solidi (b) **136**, 167 (1986).
- <sup>38</sup> L. M. Sandratskii, J. Phys.: Condens. Matter **3**, 8565 (1991).
- <sup>39</sup> A. R. Williams, J. Kübler, and C. D. Gelatt, Phys. Rev. B **19**, 6094 (1979).
- <sup>40</sup> V. Eyert, *The Augmented Spherical Wave Method, Lecture Notes in Physics* **849**, (Springer-Verlag Berlin Heidelberg 2012).
- <sup>41</sup> U. von Barth and L. Hedin, J. Phys. C **5**, 1629 (1972).
- <sup>42</sup> M. Uhl, L. M. Sandratskii, and J. Kübler, J. Magn. Magn. Mater. **103**, 314 (1992).
- <sup>43</sup> Atsushi Miyake, Leonid M. Sandratskii, Ai Nakamura, Fuminori Honda, Yusei Shimizu, Dexin Li, Yoshiya Homma, Masashi Tokunaga, and Dai Aoki, Phys. Rev. B **98**, 174436 (2018).
- <sup>44</sup> S. L. Dudarev, G. A. Botton, S. Y. Savrasov, C. J. Humphreys, and A. P. Sutton, Phys. Rev. B **57**, 1505 (1998).
- <sup>45</sup> A. V. Shubnikov and N. V. Belov, *Colored Symmetry* (Pergamon Press, Oxford, 1964).
- <sup>46</sup> W. F. Brinkman and R. J. Elliott, Proceedings of the Royal Society of London Series A **294**, 343 (1966).
- <sup>47</sup> W. Brinkman and R. J. Elliott, J. Appl. Phys. **37**, 1457 (1966).
- <sup>48</sup> A. P. Cracknell, Adv. Phys. **23**, 673 (1974).
- <sup>49</sup> A. Corticelli, R. Moessner, and P. A. McClarty, Phys. Rev. B **105**, 064430 (2022).
- <sup>50</sup> Zhenyu Xiao, Jianzhou Zhao, Yanqi Li, Ryuichi Shindou, and Zhi-Da Song, Phys. Rev. X **14**, 031037 (2024).
- <sup>51</sup> Xiaobing Chen, Jun Ren, Yanzhou Zhu, Yutong Yu, Ao Zhang, Pengfei Liu, Jiayu Li, Yuntian Liu, and Caiheng Li, and Qihang Liu, Phys. Rev. X **14**, 031038 (2024).
- <sup>52</sup> Yi Jiang, Ziyin Song, Tiannian Zhu, Zhong Fang, Hongming Weng, Zheng-Xin Liu, Jian Yang, and Chen Fang, Phys. Rev. X **14**, 031039 (2024).
- <sup>53</sup> W. Szuszkiewicz, E. Dynowska, B. Witkowska, and B. Hennion, Phys. Rev. **73**, 104403 (2006).
- <sup>54</sup> S. Wakoh and J. Yamashita, J. Phys. Soc. Jpn. **21**, 1712 (1966).
- <sup>55</sup> S. Asano and J. Yamashita, J. Phys. Soc. Jpn. **23**, 714 (1967).
- <sup>56</sup> To remind, if  $\alpha_R \mathbf{k} = \mathbf{k} + \mathbf{K}_\mu$  where  $\mathbf{K}_\mu$  is reciprocal lattice vector, it is considered as identical to  $\mathbf{k}$  and is not included in  $\{\mathbf{k}\}$ .
- <sup>57</sup> L. M. Sandratskii, R. F. Egorov, and A. A. Berdyshev, phys. stat. solidi (b) **104**, 103 (1981).
- <sup>58</sup> I. Turek, Phys. Rev. B **106**, 094432 (2022).
- <sup>59</sup> L. M. Sandratskii, Soviet Physics Journal **22**, 941 (1979).
- <sup>60</sup> The direction of the field  $\mathbf{h}$  is opposite for the magnons of the A and B types.

<sup>61</sup> The formula of the SOC is not invariant with respect to the  $\{\alpha_S|\alpha_R|\boldsymbol{\tau}\}$  operations with different  $\alpha_S$  and  $\alpha_R$ . Therefore in the relativistic case the new system obtained by trans-

formation  $\{\alpha_S|\alpha_R|\boldsymbol{\tau}\}$  is essentially different from the initial one.